Hindawi
International Journal of RF and Microwave Computer-Aided Engineering
Volume 2024, Article ID 1804375, 12 pages
https://doi.org/10.1155/2024/1804375

Research Article

A High-Gain Wideband Fabry-Pérot Antenna Employing a Water-Based Frequency Selective Surface for Polarization- and RCS-Reconfigurability

Ying Wang[1], **Zhiming Liu**[1], **Huilin Zhou**[1], **Jens Bornemann**[2], **Yuhao Wang**[1] and **Xiangkun Kong**[3]

[1]*School of Information Engineering, Nanchang University, Nanchang 330031, China*
[2]*Department of Electrical and Computer Engineering, University of Victoria, Victoria, BC, Canada V8W 2Y2*
[3]*College of Electronic and Information Engineering, Nanjing University of Aeronautics and Astronautics, Nanjing 210016, China*

Correspondence should be addressed to Zhiming Liu; zhimingliu@ncu.edu.cn

Received 19 June 2023; Revised 13 November 2023; Accepted 14 December 2023; Published 10 January 2024

Academic Editor: Lu Guo

A Fabry-Pérot (FP) antenna with wideband dual-polarization and radar cross section- (RCS-) reconfigurability adopting water-based frequency selective surface (FSS) is presented. The feed antenna is designed to switch between horizontal polarization (HP) and vertical polarization (VP) by controlling the on/off states of two PIN diodes. By optimizing the height of the FP resonant cavity, the proposed FP antenna achieves wideband and high-gain properties. In addition, the incident wave can be absorbed when the polymethyl methacrylate (PMMA) container is filled with water, which reduces the monostatic RCS. This design can be selected to be in stealth mode or radiation mode by injecting water into or extracting water from the water container. The measured results indicate that in stealth mode, the 10-dB RCS reduction band is from 4.5 GHz to 6.4 GHz, and the peak RCS reduction is 31.5 dB at 5.2 GHz. In the radiation mode, the realized gains of the FP antenna in both HP and VP at 5.2 GHz reach 16.6 dBi. Simulated and measured results verify the realizability and operational concept of the designed FP antenna.

1. Introduction

Fabry-Pérot (FP) antennas, also known as partially reflecting surface (PRS) antennas, have attracted a high level of attention among antenna researchers due to their simple feeding structure, highly directive radiation pattern, and high-gain performance [1–3]. The array antenna can also be used to effectively improve the gain of the antenna, but the array antenna has obvious shortcomings such as complex feeding network [4]. FP antennas typically consist of a feed antenna, and a PRS. From the ray theory, the FP antenna can achieve significant gain enhancement by making full use of the electromagnetic characteristics of PRS.

Polarization reconfigurable antennas also have a very wide range of application scenarios such as suppressing fading losses and enhancing the capacity of wireless communications [5–7]. In practical applications, many FP antennas with polarization reconfigurable performance have been proposed [8–10]. It is not only possible to realize the FP antenna's reconfigurability by changing the feed antenna, but also to achieve reconfiguration by controlling the PRS [11, 12]. Also, the direction of polarization of the antenna can be controlled by adding semiconductor devices, such as p-i-n diode and varactor diode [13, 14]. Moreover, FP antennas have good applications in high-frequency bands, including the millimeter-wave band. References [15, 16] demonstrate the successful utilization of 3D printing materials for manufacturing antennas, resulting in impressive radiation performance.

In recent years, there has been an increasing focus among researchers in the field of antenna research on reducing the RCS, alongside endeavors to expand frequency bandwidth and improve realized gain, resulting in some satisfactory progress [17, 18]. The reduction of RCS in antennas plays a crucial role in achieving stealth mode in communication devices, and it also significantly influences the stealth capabilities of defense electronic equipment [19, 20].

Several approaches have been proposed to achieve RCS reduction for FP antennas [21–29]. In [21], two PRSs based on phase gradient metasurface (PGM) were designed to realize wideband RCS reduction including both in- and out-of-band frequency regions. Ref. [22] designed a checkerboard artificial magnetic conductor (AMC) structure to reduce the RCS over a wide band. Ref. [23] makes use of the $180° \pm 37°$ reflection phase variations between adjacent FSS unit cells on the metasurface to realize RCS reduction. Polarization conversion metasurfaces (PCMs) and checkerboard-arranged metasurfaces (CAMs) can also be used to reduce the RCS [24–26]. However, these methods have the disadvantage that the reduction values of RCSs were not large enough. Besides, using absorption surfaces (ASs) can reduce RCS in a larger range, and RCS reduction values were relatively large [27]. However, low-RCS antennas with ASs absorb the radiation energy, which greatly reduces the gain of the antenna and even leads to the deterioration of the radiation pattern. These designs mentioned above can achieve outstanding RCS reduction, but they are hard to achieve its reconfigurability [21–27].

In order to solve this problem, some researches have proposed designs involving liquid absorbers [28, 29]. Liquid absorbers have the advantages of high adjustability, fluidity, and reconfigurable properties, and they will have broad application prospects. Ref. [30] achieved ultrawideband high absorptivity from 4.63 to 100 GHz using liquid water. Therefore, water-based absorbers can decrease the RCS to a greater extent. In the microwave frequency band, water has a satisfactory dielectric loss, and the permittivity of water is related to temperature [31, 32]. Through the fluidity of water, a water-based FSS can be designed to selectively reflect, transmit, or absorb certain frequencies of electromagnetic waves, allowing for flexible control over the antenna's response and RCS. Moreover, antennas incorporating water-based FSS can easily realize RCS reconfiguration characteristics. Furthermore, the high loss and ready availability of water make it stand out in achieving antenna RCS reduction compared to liquid ethanol and liquid metals which are commonly used in liquid absorbers.

In this work, a water-based FSS unit is designed to form a PRS layer of a FP antenna. The designed FP antenna exhibits favorable performance characteristics, including wideband, high gain, polarization-reconfiguration, and RCS-reconfiguration. Through measurements, the FP antenna can reach a maximum realized gain of 16.6 dBi in both the HP and VP. Meanwhile, it achieves a measured 10 dB impedance matching bandwidth ($S_{11} < -10$ dB) from 4.71 GHz to 5.53 GHz. Also, the 10 dB RCS reduction band of the FP antenna in stealth mode is from 4.5 GHz to 6.5 GHz (36.4%), which is located within the C-band (4-8 GHz), and some radar and satellite communication designs have been applied in this operating frequency band [33–35]. The experimental results demonstrate that the antenna exhibits noteworthy performance metrics. This paper serves as an extension and continuation of our previously published work [36].

2. Water-Based FSS and Feed Antenna

2.1. Water-Based FSS Unit. The water-based FSS unit is a three-layer structure that can be decomposed into a polymethyl methacrylate (PMMA) container, a water layer, and a bottom F_4BM265 substrate ($\varepsilon_r = 2.65$, $\tan\delta = 0.0007$) with an etched square metal patch. The designed water-based FSS unit is shown in Figure 1(a). The container is located on the top layer and made of PMMA material ($\varepsilon_r = 2.67$, $\tan\delta = 0.01$), forming a closed water storage structure with the bottom substrate. There is a groove in the middle of the container. The side length of the square at the bottom of the groove is p_1, and the height is h_{p1}. The groove is used as the water layer. Figure 1(b) shows the hierarchical structure of the unit. The edge-to-edge distance of the bottom square metal patch from the substrate is 0.4 mm.

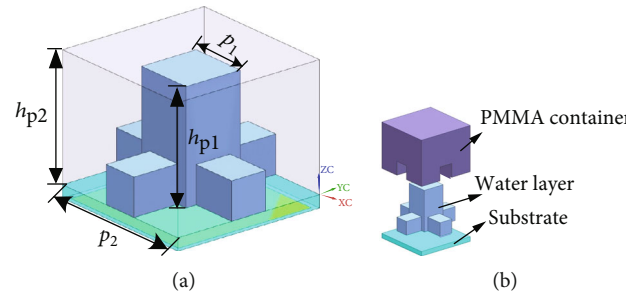

Figure 1: Model of a water-based FSS unit.

The water-based FSS unit serves as an absorber. The influence of different parameters on the absorption band is shown in Figures 2(a) and 2(b). In Figure 2(a), it is observed that h_{p1} has an effect on the absorption band, but the changes caused by this effect are acceptable. As shown in Figure 2(b), as p_1 decreases, the absorption band becomes narrower, and the value of S_{11} also decreases. However, the overall absorption band of the absorber shifts towards higher frequencies. The reason for the change of the absorption band is that different parameters will affect the impedance match between the absorber and free space.

To achieve the optimal properties of the absorber, the final parameters are obtained as $h_{p1} = 9$ mm, $h_{p2} = 10$ mm, $p_1 = 4.8$ mm, and $p_2 = 12.5$ mm. Figure 3(a) shows the simulated model of the water-based FSS unit. As shown in Figure 3(b), comparing S_{11} of the FSS unit with and without water, it can be found that S_{11} decreases significantly after water injection. The absorption band ($S_{11} < -10$ dB) is from 3.8 GHz to 6.5 GHz. From Figure 3(c), it can be observed that the absorptivity of the FSS unit exceeds 90% in the range of 4.77 GHz to 6.45 GHz, with a maximum value of approximately 98.5% at 5.5 GHz.

2.2. Feed Antenna. Figure 4 shows the schematic diagram of the slot-coupled patch antenna (i.e., feed antenna). The required parameters are summarized in Table 1. The linear polarizations in two orthogonal directions are realized by two perpendicularly positioned H-shaped slots etched on the ground plane. The feed lines are printed on the bottom of substrate 1. And the polarization direction of the antenna is controlled by two PIN diodes labeled as PIN 1 and PIN 2. The two PIN diodes are soldered into the feedlines. If PIN 1 is forward biased and PIN 2 is reverse biased, the antenna radiates vertical polarized waves. Similarly, if PIN 2 is

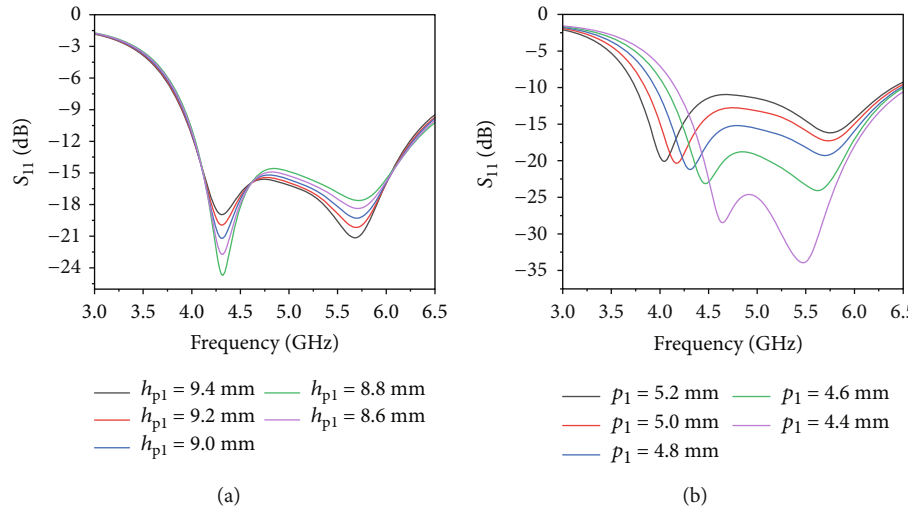

FIGURE 2: S_{11} of the water-based FSS with different values of (a) height h_{p1} and (b) width p_1.

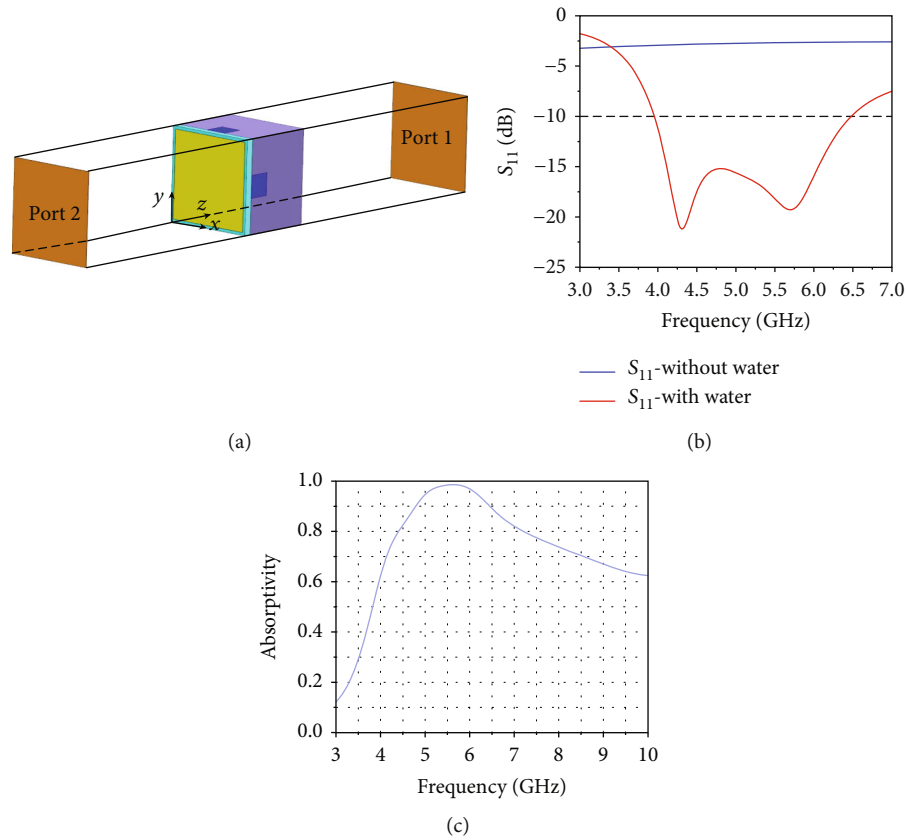

FIGURE 3: (a) Simulated model of a water-based FSS unit, (b) simulated S_{11} of FSS unit with and without water, and (c) simulated absorptivity.

forward biased and PIN 1 is reverse biased, the antenna radiates horizontal polarized waves. Also, in order to further widen the antenna's operating bandwidth, a square metal patch is printed on the top of substrate 2. Both layers of dielectric substrate are F_4BM265 material.

Figures 5(a) and 5(b) show the simulated S_{11} and realized gain of the dual-polarized feed antenna. For this case, the feed antenna has a common 10 dB return loss bandwidth of 5-5.7 GHz and a maximum realized gain of 8.7 dBi at 5.6 GHz for both HP and VP. In Figure 5(a), it can be found that even though the 10 dB impedance bandwidths are almost the same in both horizontal and vertical polarizations, there are still some deviations in $|S_{11}|$ values. This difference is caused by the H-shaped slots etched on the ground plane. This is because there is a modest deviation between the positions of the H-shaped slots corresponding to different polarizations, which

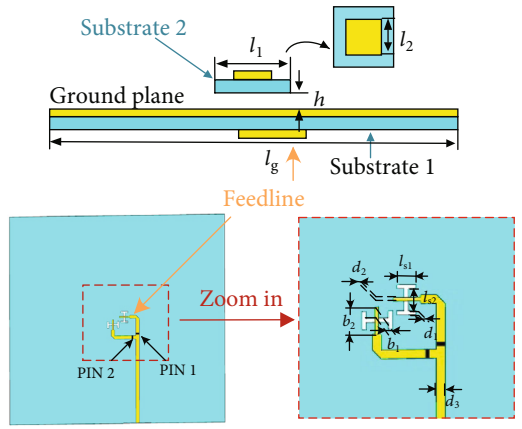

Figure 4: Structural diagram of the feed antenna.

Table 1: Parameters of the proposed antenna.

Parameters	l_g	l_1	l_2	h
Value (mm)	157.0	30.0	17.7	3.1
Parameters	b_1	b_2	b_3	d_1
Value (mm)	3.0	7.7	4.4	1.2
Parameters	d_2	d_3	l_{s1}	l_{s2}
Value (mm)	1.0	2.5	5.2	6.2

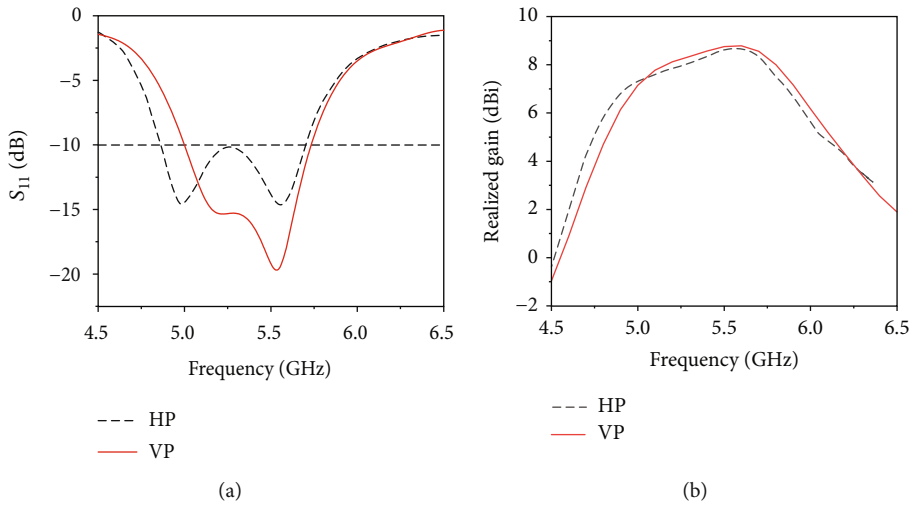

Figure 5: Simulated results of the feed antenna. (a) S_{11} and (b) realized gain.

affects the distribution of electromagnetic waves. Figure 5(b) shows that the realized gains in two polarizations are nearly the same.

3. Reconfigurable FP Antenna

3.1. FP Antenna in Radiation Mode. The characteristics of the FP antenna are closely related to the height of the FP cavity. The resonance equation of the FP antenna is as follows:

$$\varphi_{\text{prs}} = \frac{4\pi h}{\lambda} - \varphi_g + 2n\pi, \quad n = 0, 1, 2, \cdots, \tag{1}$$

where h is the height of the FP cavity. Additionally, φ_{prs} and φ_g, respectively, represent the reflection phases of the PRS layer and ground plane. When the reflection properties of PRS and cavity height satisfy Equation (1), the FP resonant mode can be excited to achieve gain enhancement.

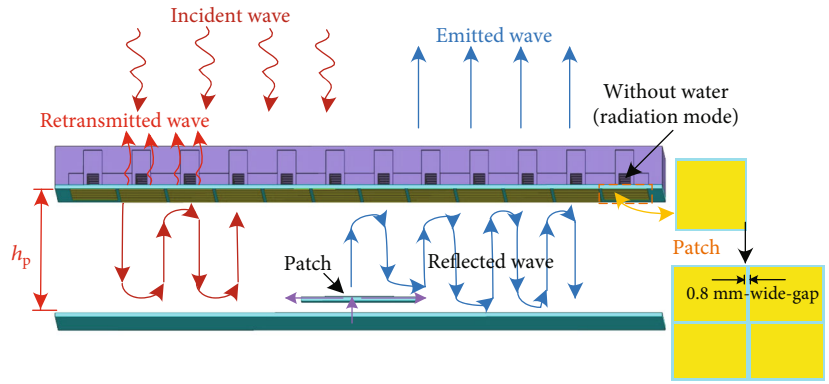

Figure 6: Working schematic diagram in radiation mode.

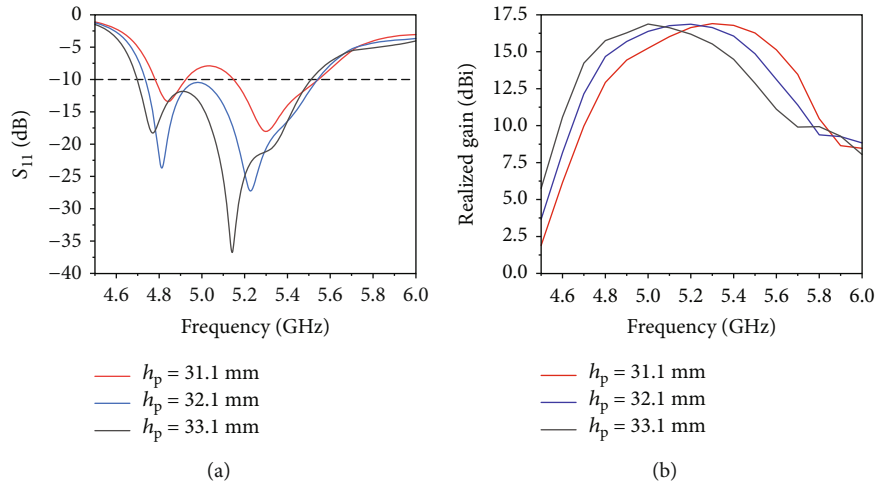

Figure 7: Simulated results of the FP antenna with different h_p. (a) S_{11} and (b) realized gain.

FP antenna consists of a feed antenna and a PRS layer. In this design, the PRS layer adopts the water-based FSS unit mentioned in Section 2. The antenna uses 12 × 12 FSS units to form the PRS layer. Figure 6 shows the working schematic diagram of the FP antenna. The spacing between the square metallic patches located at the bottom of the PRS is 0.8 mm. The incident wave can be partially reflected through the metal patch and the gap between them, thus increasing the gain. The height of the cavity has a significant impact on the resonance conditions. Figures 7(a) and 7(b) compare S_{11} and realized gain at different heights of the cavity. According to Figure 7, when the height of h_p changes, the simulated S_{11} and realized gain are obviously different. The simulated results verify the above statements.

When h_p = 31.1 mm, the simulated S_{11} curve moves up significantly, and the 10 dB operating band is greatly reduced. Moreover, although the simulated S_{11} of the FP antenna has a common 10 dB operating band when h_p = 32.1 mm and h_p = 33.1 mm, the frequency point corresponding to the gain peak can have a larger offset when h_p = 33.1 mm. This is due to the change of cavity resonant frequency caused by the change of cavity height. Considering the comprehensive performance of the FP antenna, the realized gain

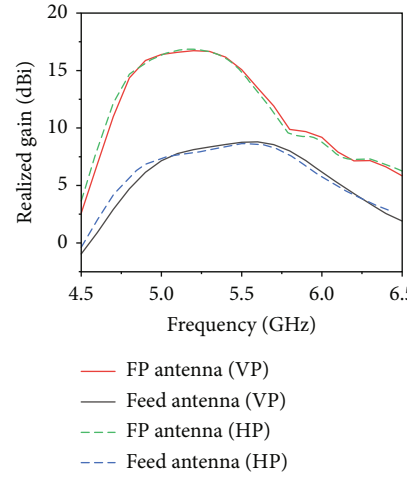

Figure 8: Realized gain of FP antenna and feed antenna.

of the FP antenna reaches 16.9 dBi in HP and 16.7 dBi in VP at 5.2 GHz when h_p = 32.1 mm. Figure 8 compares the realized gain of the feed antenna and FP antenna. It can be observed that the realized gain of the FP antenna increases

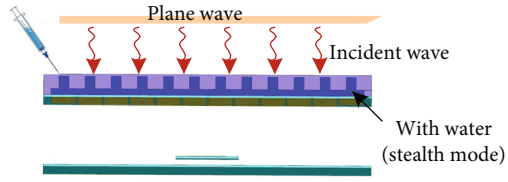

Figure 9: Working schematic diagram in stealth mode.

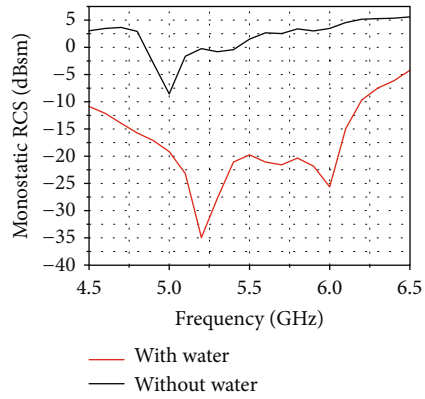

Figure 10: Simulated monostatic RCSs with/without liquid water.

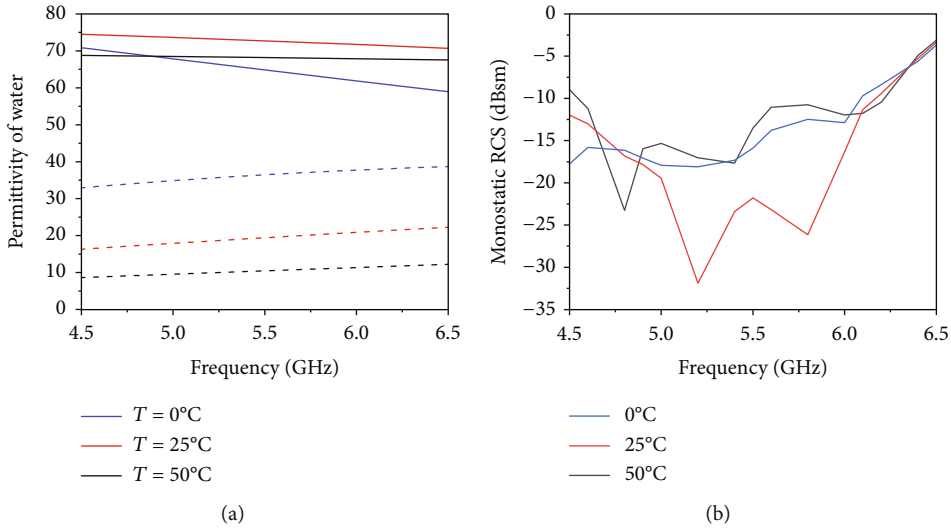

Figure 11: (a) Permittivity of water. (b) Simulated monostatic RCS reduction curves of the FP antenna at different temperatures.

by more than 5 dB compared to the feed antenna in the frequency range of 4.5 GHz to 5.6 GHz. At 5.2 GHz, the peak gain enhancement within the operating band is increased by 9 dB, which shows a superior high-gain performance of the FP antenna.

3.2. FP Antenna in Stealth Mode. The simulated results of the designed FSS unit show that the FSS unit has considerable absorptivity, which lays a good theoretical foundation for the FP antenna to realize stealth mode. In this design, a method is presented to achieve a reconfigurable RCS by injecting water into and extracting water from the PRS layer. After water injection, the working schematic diagram of RCS reduction is depicted in Figure 9. The incident wave can be absorbed by the PRS layer rather than reflected in other directions when the PMMA container is filled with water.

The simulated monostatic RCS of the proposed FP antenna with and without water injection in the PMMA container are shown in Figure 10. It can be observed that the simulated monostatic RCS of the proposed antenna is reduced by more than 10 dB between 4.5 GHz and 6.5 GHz, with a maximum RCS reduction of 35 dB at 5.2 GHz. Since the temperature can affect the permittivity of water, the RCS reduction curves of the antenna at different temperatures are shown in Figure 11. It can be found that RCS reduction bands of the antenna are similar at 0°C, 25°C,

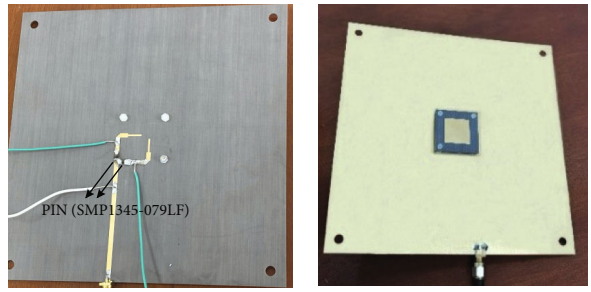

(a) (b)

FIGURE 12: Fabricated prototype of the feed antenna. (a) Bottom and (b) top.

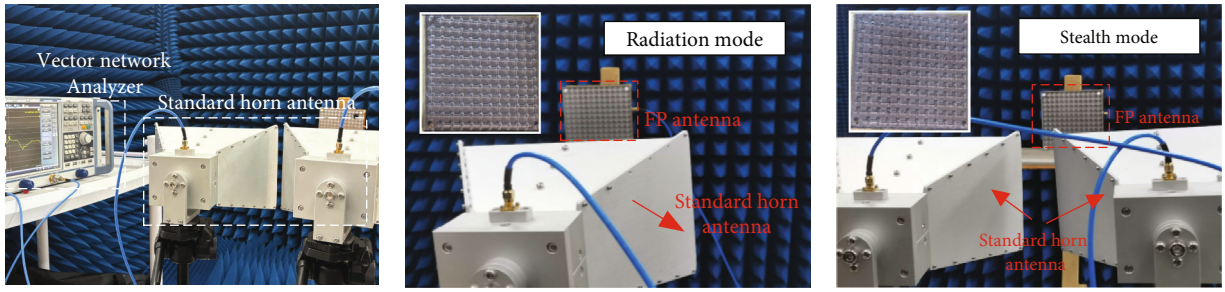

(a) (b) (c)

FIGURE 13: (a) Photograph of the experimental environment, (b) radiation mode, and (c) stealth mode.

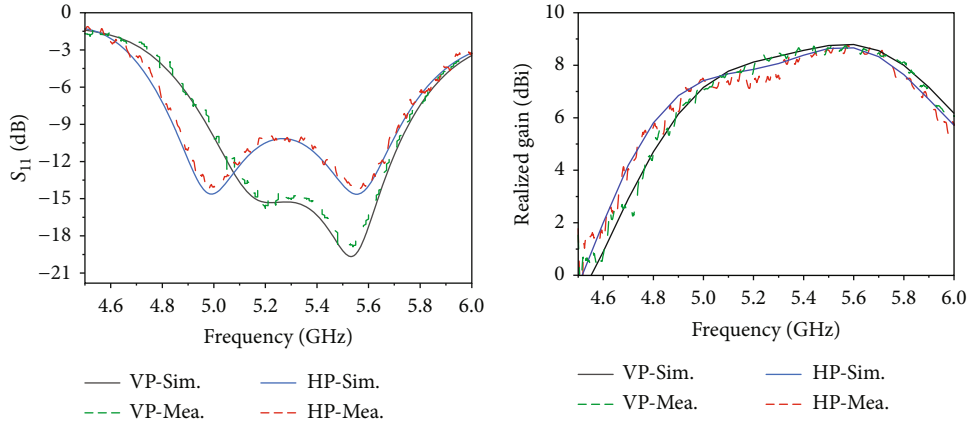

(a) (b)

FIGURE 14: Comparisons of measured and simulated results of the feed antenna. (a) S_{11} and (b) realized gain.

and 50°C, but it would be the best at 25°C. The simulated results show that the proposed antenna can effectively reduce RCS in stealth mode.

4. Fabrication and Measurement

To demonstrate the reliability of the above design, the antenna has been fabricated and measured. The PRS layer is mounted over the ground plane with a height of h_p using nylon screws and nuts. As shown in Figure 12, the feed antenna is printed on a 1 mm-thick F_4BM265 ($\varepsilon_r = 2.65$, $\tan\delta = 0.0007$) substrate. The measurements of the fabricated antenna were completed in the experimental environment shown in Figure 13. A pair of standard horn antennas and a vector network analyzer are used to complete the measurement in the microwave anechoic chamber.

The measured results in Figure 14 show that the feed antenna has 10 dB impedance bandwidths of 4.87-5.69 GHz and 5.00-5.72 GHz, and maximum realized gains of 8.56 dBi and 8.71 dBi, respectively, at 5.6 GHz for HP and VP. Figure 15 shows the S_{11} and the realized gain of the FP antenna without water for horizontally and vertically polarized waves. According to the results in Figure 15, the FP antenna has a common measured 10 dB impedance bandwidth of 4.71-5.53 GHz, and a maximum gain of 16.6 dBi at 5.2 GHz.

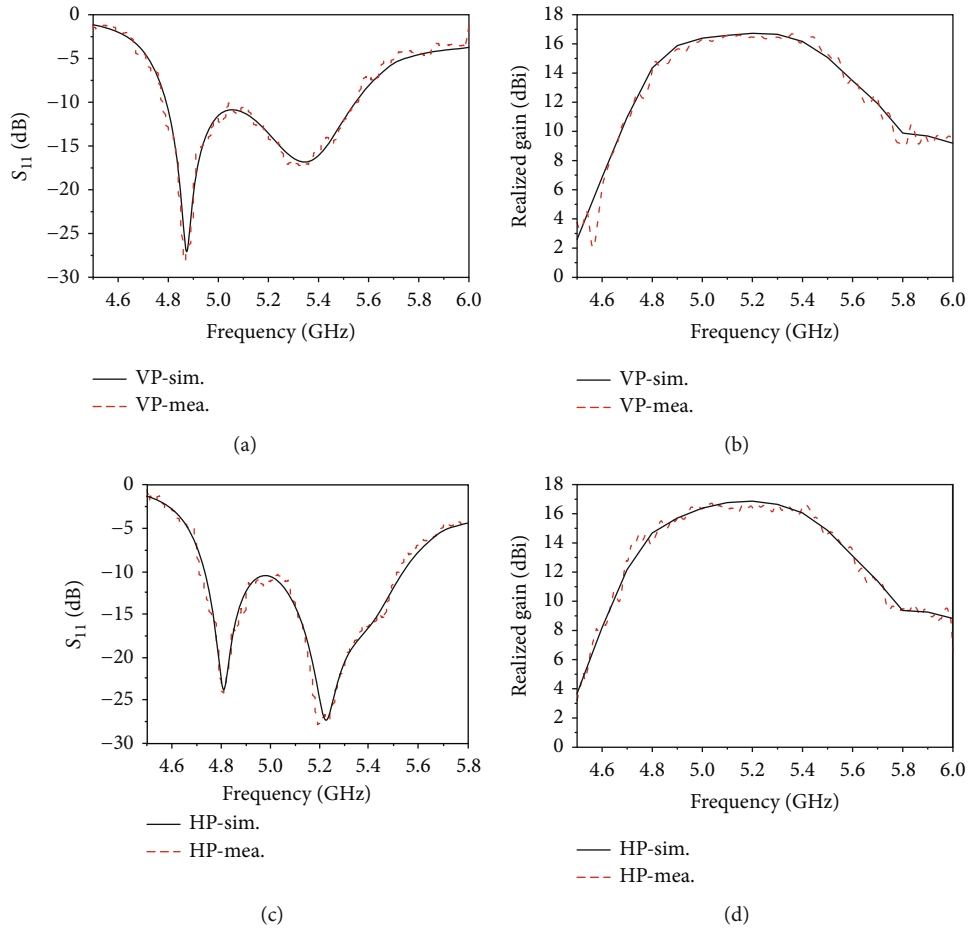

FIGURE 15: Comparisons of measured and simulated results of the FP antenna. (a) S_{11} for VP, (b) realized gain for VP, (c) S_{11} for HP, and (d) realized gain for HP.

Figure 16 shows the monostatic RCS of the antenna with and without water. Due to machining errors of components and the inability to remove all air bubbles when water is injected into the PMMA container, it is difficult to achieve complete consistency between the measured results and the simulated results. We randomly placed some bubbles of different sizes in the water layer to simulate the possible errors in the measurement. The measured results show that even in the presence of unavoidable external factors such as bubbles, the antenna can still significantly reduce the RCS. Obviously, the measured results are similar to the simulated results, and both of them show superior RCS reduction performance.

Figure 17 shows the measured and simulated co-and cross-polarization radiation patterns of the proposed FP antenna in the E- and H-planes at 4.8 GHz, 5.1 GHz, and 5.4 GHz. The measured results are in good proximity with simulations and illustrate that the antenna has superior radiation characteristics in the operating band.

Table 2 lists some performances of this antenna and other works. It can be seen that this design is a compromise solution. By utilizing the RCS reconfigurable performance of the antenna, it is aimed at balancing the performance in radiation and stealth modes, enabling it to perform well in both modes. It shows that the proposed antenna has excellent 10 dB impedance bandwidth, gain enhancement, and 10 dB RCS reduction band. The measured results are close to the simulated results, reflecting the realizability of the antenna.

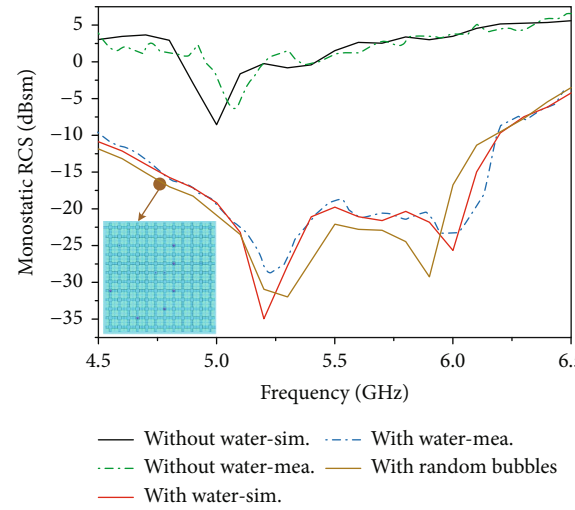

FIGURE 16: Simulated and measured monostatic RCS of the antenna with/without water or with random bubbles.

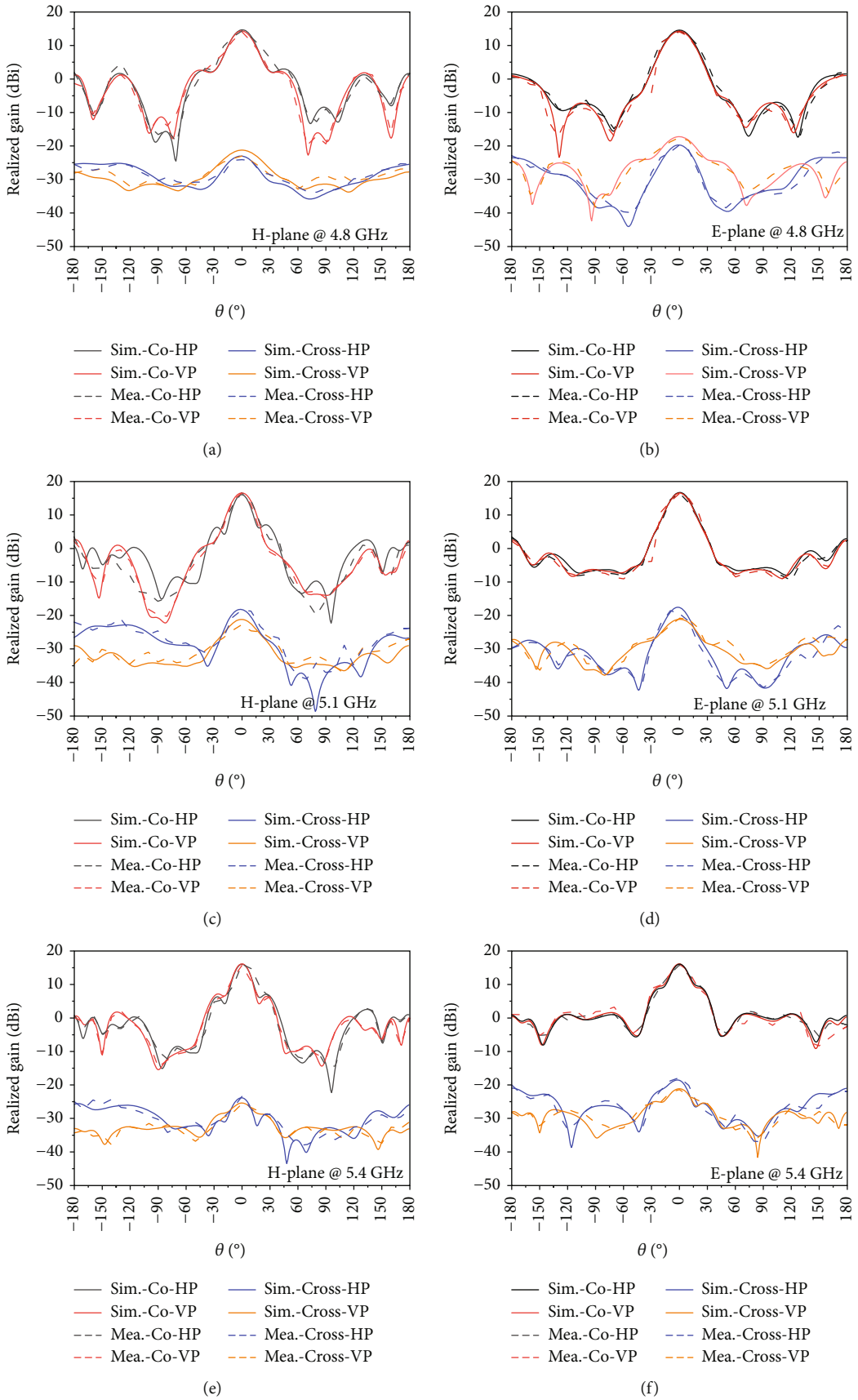

Figure 17: Simulated and measured co- and cross-polarization radiation patterns of the proposed antenna. (a) H-plane at 4.8 GHz, (b) E-plane at 4.8 GHz, (c) H-plane at 5.1 GHz, (d) E-plane at 5.1 GHz, (e) H-plane at 5.4 GHz, and (f) E-plane at 5.4 GHz.

Table 2: Comparison between the designed antenna and existed works.

Ref.	Method	RCS reconfiguration	Pol. mode	10 dB impedance bandwidth (GHz)	Max. realized gain (dBi)	10 dB RCS reduction band (GHz)	Max. RCS reduction value (dB)	Area (λ_0^2)
[2]	Electronic control	No	Dual-linear	2.20-2.72 (21.1%)	15.1 (HP) 14.8 (VP)	N.A.	N.A.	1.4×1.4
[17]	CAM	No	Single-linear	8.64-12.07 (33.1%)	17.1	About 10.1-11.8 (15.5%)	19.5	2.8×2.8
[18]	AS	No	Circularly polarized	10.50-10.78 (2.6%)	About 9.5	About 5.8-8.2 (33.8%) +10.7-10.9 (1.9%)	27.6	2.7×2.7
[26]	CAM	No	Single-linear	9.42-11.35 (18.6%)	About 12.0	9.6-16.9 (55.1%)	39.4	2.2×2.2
[28]	Liquid absorber	Yes	Single-linear	About 2.98-3.12 (4.6%)	12.1	About 7.3-17.6 (82.7%)	36.0	1.2×2.2
This work	Water-based FSS+ electronic control	Yes	Dual-linear	4.71-5.53 (16.0%)	16.6 (both HP and VP)	4.5-6.5 (36.4%)	30.8	2.7×2.7

Note: λ_0 denotes the wavelength at the center frequency of the effective bandwidth in free space.

5. Conclusions

An RCS-reconfigurable dual-polarization FP antenna using water-based FSS is proposed. Through two PIN diodes, this antenna can switch between horizontal and vertical polarization. The maximum gain enhancement can reach up to 9 dB compared to the feed antenna. Compared with the feed antenna, the realized gain increased by a maximum of 9 dB after adopting the FP resonant cavity. The results show that the designed FP antenna has a common measured 10 dB return loss bandwidth from 4.71 GHz to 5.53 GHz for both HP and VP. The peak realized gain is 16.6 dBi at 5.2 GHz. In addition, the RCS reconfigurability of the proposed antenna can be flexibly achieved by injecting water into and extracting water from the PMMA container. The results show that the monostatic RCS has a maximum reduction of 30.8 dB after water injection. The 10 dB RCS reduction band is from 4.5 GHz to 6.4 GHz which includes the operating frequency band in radiation mode. The simulated and measured results indicate that the proposed antenna exhibits excellent radiation performance and RCS reconfiguration capability.

Data Availability

The data are available on request from the authors.

Conflicts of Interest

The authors declare that they have no conflicts of interest.

Acknowledgments

This work was supported by the National Natural Science Foundation of China (Grant numbers 62201240, 62161027, and 62061030), the Open Fund of the key laboratory of radar imaging and microwave photon technology of the Ministry of Education (Grant number NJ20220005), the Jiangxi Provincial Natural Science Foundation (Grant number 20224BAB212005), and Open research project of the science and technology innovation platform (Huaqiao University) of Fujian Key Laboratory of Special Energy Manufacturing (Grant number FKLSEM-2022-04).

References

[1] A. P. Feresidis and J. C. Vardaxoglou, "High gain planar antenna using optimised partially reflective surfaces," *IEE Proceedings-Microwaves, Antennas and Propagation*, vol. 148, no. 6, pp. 345–350, 2001.

[2] R. Lian, Z. Tang, and Y. Yin, "Design of a broadband polarization-reconfigurable Fabry–Perot resonator antenna," *IEEE Antennas and Wireless Propagation Letters*, vol. 17, no. 1, pp. 122–125, 2018.

[3] Z. G. Liu, Z. X. Cao, and L. N. Wu, "Compact low-profile circularly polarized Fabry–Perot resonator antenna fed by linearly polarized microstrip patch," *IEEE Antennas and Wireless Propagation Letters*, vol. 15, pp. 524–527, 2016.

[4] M. Asaadi and A. Sebak, "Gain and bandwidth enhancement of 2 × 2 square dense dielectric patch antenna array using a holey superstrate," *IEEE Antennas and Wireless Propagation Letters*, vol. 16, pp. 1808–1811, 2017.

[5] S. Gao, A. Sambell, and S. S. Zhong, "Polarization-agile antennas," *IEEE Antennas and Propagation Magazine*, vol. 48, no. 3, pp. 28–37, 2006.

[6] M. S. Smith and L. Neal, "A comparison of polarization and space diversity for indoor propagation at 900 MHz," in *Proceedings of 2nd IEEE International Conference on Universal Personal Communications*, pp. 74–78, Ottawa, Canada, 1993.

[7] Y. Sung, "Dual-band reconfigurable antenna for polarization diversity," *International Journal of Antennas and Propagation*, vol. 2018, Article ID 6878607, 7 pages, 2018.

[8] Y.-G. Jeon, G.-R. Yun, and D. Kim, "A new design of a Fabry-Perot cavity antenna for Beam-scanning with polarization-reconfiguration," in *2022 International symposium on antennas and propagation (ISAP)*, pp. 423-424, Sydney, Australia, 2022.

[9] Y. Wang and A. Zhang, "Dual circularly polarized Fabry–Perot resonator antenna employing a polarization conversion metasurface," *IEEE Access*, vol. 9, pp. 44881–44887, 2021.

[10] S. Zhu, J. He, J. Yu, Y. Feng, S. Pan, and G. Li, "Tri-polarization reconfigurable Fabry-Perot resonator antenna in Ku-band," *The Applied Computational Electromagnetics Society Journal (ACES)*, vol. 37, no. 8, pp. 848–855, 2023.

[11] P. Xie, G. Wang, T. Cai, H. Li, and J. Liang, "Novel Fabry-Pérot cavity antenna with enhanced beam steering property using reconfigurable meta-surface," *Applied Physics A*, vol. 123, no. 7, pp. 1–6, 2017.

[12] S. Das and S. Sahu, "Polarization reconfigurability enabled metamaterial inspired dielectric resonator based Fabry-Perot resonator cavity antenna with high gain and bandwidth," *International Journal of RF and Microwave Computer-Aided Engineering*, vol. 31, no. 5, Article ID e22603, 2021.

[13] S. K. Saraswat and A. R. Harish, "Dual-band polarisation reconfigurable grounded fractal slot antenna," *IET Microwaves, Antennas & Propagation*, vol. 14, no. 14, pp. 1786–1790, 2020.

[14] M. Suresh Kumar and Y. K. Choukiker, "Tunable wideband frequency and switching polarisation reconfiguration antenna for wireless applications," *IET Microwaves, Antennas & Propagation*, vol. 12, no. 15, pp. 2364–2371, 2018.

[15] Q.-Y. Guo, Q. W. Lin, and H. Wong, "A high gain millimeter-wave circularly polarized Fabry–Pérot antenna using PRS-integrated polarizer," *IEEE Transactions on Antennas and Propagation*, vol. 69, no. 2, pp. 1179–1183, 2021.

[16] F. Wu and K. M. Luk, "Circular polarization and reconfigurability of Fabry–Pérot resonator antenna through metamaterial-loaded cavity," *IEEE Transactions on Antennas and Propagation*, vol. 67, no. 4, pp. 2196–2208, 2019.

[17] Z. Liu, S. Liu, X. Zhao, X. Kong, Z. Huang, and B. Bian, "Wideband gain enhancement and RCS reduction of Fabry–Perot antenna using hybrid reflection method," *IEEE Transactions on Antennas and Propagation*, vol. 68, no. 9, pp. 6497–6505, 2020.

[18] J. Ren, W. Jiang, K. Zhang, and S. Gong, "A high-gain circularly polarized Fabry–Perot antenna with wideband low-RCS property," *IEEE Antennas and Wireless Propagation Letters*, vol. 17, no. 5, pp. 853–856, 2018.

[19] E. F. Knott, J. F. Shaeffer, and M. T. Tuley, *Radar Cross Section*, Sci Tech, Raleigh, NC, USA, 2004.

[20] T. Hong, K. Peng, G. Yue, W. Jiang, and S. Gong, "Wideband polarization conversion metasurface for RCS reduction of antennas," *International Journal of Antennas and Propagation*, vol. 2018, Article ID 2308643, 8 pages, 2018.

[21] Y. Jia, Y. Liu, W. Zhang, J. Wang, S. Gong, and G. Liao, "High-gain Fabry-Pérot antennas with wideband low monostatic RCS using phase gradient metasurface," *IEEE Access*, vol. 7, pp. 4816–4824, 2018.

[22] D. Sang, Q. Chen, L. Ding, M. Guo, and Y. Fu, "Design of checkerboard AMC structure for wideband RCS reduction," *IEEE Transactions on Antennas and Propagation*, vol. 67, no. 4, pp. 2604–2612, 2019.

[23] S. Zarbakhsh, M. Akbari, F. Samadi, and A. R. Sebak, "Broadband and high-gain circularly-polarized antenna with low RCS," *IEEE Transactions on Antennas and Propagation*, vol. 67, no. 1, pp. 16–23, 2019.

[24] J. Ren, W. Jiang, and S. Gong, "Low RCS and broadband metamaterial-based low-profile antenna using PCM," *IET Microwaves, Antennas & Propagation*, vol. 12, no. 11, pp. 1793–1798, 2018.

[25] M. Long, W. Jiang, and S. Gong, "Wideband RCS reduction using polarization conversion metasurface and partially reflecting surface," *IEEE Antennas and Wireless Propagation Letters*, vol. 16, pp. 2534–2537, 2017.

[26] Y. Zheng, J. Gao, Y. Zhou et al., "Wideband gain enhancement and RCS reduction of Fabry–Perot resonator antenna with chessboard arranged metamaterial superstrate," *IEEE Transactions on Antennas and Propagation*, vol. 66, no. 2, pp. 590–599, 2018.

[27] J. Mu, H. Wang, H. Wang, and Y. Huang, "Low-RCS and gain enhancement design of a novel partially reflecting and absorbing surface antenna," *IEEE Antennas and Wireless Propagation Letters*, vol. 16, pp. 1903–1906, 2017.

[28] Y. Zou, X. Kong, L. Xing et al., "A slot antenna array with reconfigurable RCS using liquid absorber," *IEEE Transactions on Antennas and Propagation*, vol. 70, no. 7, pp. 6095–6100, 2022.

[29] G. Deng, T. Xia, S. Jing, J. Yang, H. Lu, and Z. Yin, "A tunable metamaterial absorber based on liquid crystal intended for F frequency band," *IEEE Antennas and Wireless Propagation Letters*, vol. 16, pp. 2062–2065, 2017.

[30] X. Kong, L. Kong, S. Jiang, X. Wang, Y. Zou, and L. Xing, "Low-profile and dual-polarization water-based frequency selective rasorber with ultrawideband absorption," *IEEE Antennas and Wireless Propagation Letters*, vol. 20, no. 12, pp. 2534–2538, 2021.

[31] C. Hua, S. Wang, Z. Hu et al., "Reconfigurable antennas based on pure water," *IEEE Open Journal of Antennas and Propagation*, vol. 2, pp. 623–633, 2021.

[32] X. Yan, X. Kong, Q. Wang et al., "Water-based reconfigurable frequency selective rasorber with thermally tunable absorption band," *IEEE Transactions on Antennas and Propagation*, vol. 68, no. 8, pp. 6162–6171, 2020.

[33] C. J. Baker, F. Ahmad, A. DeMaio et al., *IEEE Standard Letter Designations for Radar-Frequency Bands-Redline*, IEEE Std 521-2019 (Revision of IEEE Std 521-2002) - Redline, 2020, https://ieeexplore.ieee.org/document/9027205.

[34] E. Asihene, D. S. Desmond, M. L. Harasyn et al., "Toward the detection of oil spills in newly formed sea ice using C-band multipolarization radar," *IEEE Transactions on Geoscience and Remote Sensing*, vol. 60, pp. 1–15, 2022.

[35] C. Li, Y. Xiao, and J. Lin, "A 5GHz double-sideband radar sensor chip in 0.18μm CMOS for non-contact vital sign detection," *IEEE Microwave and Wireless Components Letters*, vol. 18, no. 7, pp. 494–496, 2008.

[36] Y. Wang, Z. Liu, H. Zhou, Y. Wang, and Z. Wang, "Wideband high-gain Fabry-Pérot antenna with polarization- and RCS-reconfigurable employing water-based FSS," in *2023 International Conference on Microwave and Millimeter Wave Technology (ICMMT)*, pp. 1–3, Qingdao, China, 2023.